A Comparative Study of the Preamplifiers in Electrostatic Sensors through Analytical Modelling and Experimental Evaluation

Yonghui Hu, *Senior Member*, *IEEE*, Yong Yan, *Fellow, IEEE,* and Yuanqing Yang

***Abstract*—Electrostatic sensors have been used to monitor a diverse range of processes and systems that involve movement of charged objects. Several types of preamplifiers are available for signal conditioning of electrostatic sensors, which differ in many aspects. This paper presents a comprehensive comparative study of four types of preamplifiers, namely trans-resistance amplifier, charge amplifier, current sense amplifier and potential amplifier, in order to clarify their differences for correct selection and facilitate proper cabling and electrode design. An equivalent circuit model that quantifies the interaction between the charged object and the electrode using coupling capacitance is established. The voltage outputs of the four preamplifiers are expressed analytically using the potential of the charged object and the object-electrode capacitance that varies as the object moves. In order to produce repeatable and controllable inputs to the electrostatic sensor, a fluctuating electric field is actively generated by applying an excitation voltage signal on an emitting electrode. Under impulse excitation, similarities in the signal waveforms are found between the trans-resistance and current sense amplifiers as well as between the charge and potential amplifiers, apart from the opposite polarities. Both impulse and frequency responses show that the current sense and potential amplifiers are significantly affected by the parasitic capacitances that depend on electrode structure and cabling and measures should be taken to reduce their effects.**

***Index Terms*—Electrostatic sensor, equivalent circuit model, frequency response, impulse response, preamplifier.**

I. Introduction

TRIBOCHARGING is a ubiquitous phenomenon in which electrostatic charges are generated when two materials are brought into contact and then separated. The electric shocks experienced when touching a metal doorknob in winter and the attraction of tiny pieces of paper to a plastic comb rubbed with dry hair are examples of tribocharging in our daily lives. In industry, this phenomenon is also widely seen, e.g. particle charging during bulk solids handling and processing [1], and charge accumulation on the outer surfaces of aircrafts and projectiles in flight [2, 3]. The mechanism of charge generation entails that the charged object is engaged in some form of movement. As a result, the electric field in the vicinity of the charged object is perturbed. An electrostatic sensor that works on the principle of electrostatic induction can respond to the fluctuation of the electric field. Then information regarding the charged object can be inferred from the resulting signal. Due to the widespread occurrence of tribocharging, electrostatic sensors have been used in a diverse range of applications, including measurement of gas–solid two-phase flow, condition monitoring of mechanical systems, human activity monitoring, etc. Ref. [4] provides a comprehensive summary of the latest development of electrostatic sensors and their applications.

An electrostatic sensor mainly consists of an insulated metal electrode for passive electric field sensing and a signal conditioning circuit that brings the weak electrode signal into a voltage signal suitable for processing by data acquisition equipment. The essential part of the signal conditioning circuit is the front-end preamplifier, which can manipulate the electrode signal in different ways. In most cases, the electrode is driven to a fixed electric potential (usually the ground potential or the reference input voltage of an operational amplifier) either directly [5-8] or via a resistor [9,10]. The fluctuation of the electric field gives rise to variation of the induced charge on the electrode. Either a current-sensitive or a charge-sensitive preamplifier can convert the induced signal into a voltage signal. For gas–solid two-phase flow measurement, the induced current signal has been used extensively to measure particle velocity, concentration and mass flowrate [6, 9, 10]. Hu *et al*. [11, 12] measured the transverse vibration of power transmission belts using both the induced charge and induced current signals. It was found that the induced charge signal reflects the transverse displacement of the belt, whereas the induced current signal is related to the transverse velocity.

The electrode can also be electrically floating. Then the potential of the electrode varies due to capacitive coupling between the electrode and the moving charged object as well as the stray capacitance between the electrode and the ground. A voltage buffer preamplifier can be used to convert the high impedance signal from the electrode to a low impedance signal.

Manuscript received Month xx, 20xx; revised Month xx, 20xx; accepted Month xx, 20xx. This work was supported by the National Natural Science Foundation of China under Grant 61973115. (*Corresponding author: Yong Yan*.)

Y. Hu and Y. Yang are with the School of Control and Computer Engineering, North China Electric Power University, Beijing 102206, China (e-mail: huyhui@gmail.com, yangyuanqing@189.cn).

Y. Yan is with the School of Engineering, University of Kent, Canterbury, Kent CT2 7NT, UK (phone: 00441227823015; fax: 00441227456084; e-mail: y.yan@kent.ac.uk).

Gajewski [13] modelled the particle flow measuring device as a three-electrode system consisting of a charged particle, a ring probe and a grounded metal screen. The probe potential was derived using an equivalent circuit model of the three-electrode system. Wang *et al*. [14] detected the direction of hand motion using a preamplifier circuit that buffers the electrode potential developed by the induced charge on the input capacitance of an operational amplifier. Browning *et al*. [15] investigated the detection of rapidly moving charged projectiles using a free-space electric potential sensor, which was so named because a potential measuring preamplifier was employed. Actually, potential sensors are extensively used in the field of biomedical engineering to detect electrical activities of human brains, hearts and muscles [16], where the varying electric field is caused by the physiological process of human bodies rather than moving charged objects.

The above review shows that there exist several types of preamplifiers for signal conditioning of electrostatic sensors. The preamplifiers differ not only in the waveform of the output signal that may lead to different interpretations of the physical process [11, 12] but also some key performance metrics of the sensor such as gain, bandwidth, stability and signal-to-noise ratio. This paper conducts a comprehensive comparative study of four types of preamplifiers, namely trans-resistance amplifier, charge amplifier, current sense amplifier and potential amplifier, in order to clarify their differences and shed light on proper cabling and design of electrostatic sensors. As a major contribution of this paper, a novel equivalent circuit model that takes into account the charged object, the electrode and the preamplifier is established. Although Xu *et al*. [10], Gajewski [13] and Wang *et al*. [17] have already developed equivalent circuit models for analysis of electrostatic sensors, the model proposed in this paper is more comprehensive and allows the sensor signal to be expressed analytically in terms of the potential of the charged object and the variable capacitive coupling between the charged object and the electrode. In comparison with the conventional approach to the modelling of electrostatic sensors based on induced charge and spatial sensitivity, the proposed modelling approach facilitates analysis of the sensing characteristics and comparison of different types of preamplifiers from a theoretical viewpoint. The second contribution lies in a novel experimental method capable of producing repeatable results for quantitative comparison of the preamplifiers. Due to the vulnerability of electrostatic charge to various environmental and operational factors, it is extremely difficult to control the quantity of charge on the measured object. The proposed experimental method approaches this problem from a different angle, i.e. by controlling the electric potential of the object. Finally, the diversity of available preamplifiers has caused some misuses of the terms in the literature. For instance, Murnane *et al*. [18], Chen *et al*. [19] and Zhang *et al*. [20] termed the conditioning circuits that convert the induced current into voltage signals as charge amplifiers by mistake. It is hopeful that misconceptions and misuses of the preamplifiers could be corrected via this comparative study.

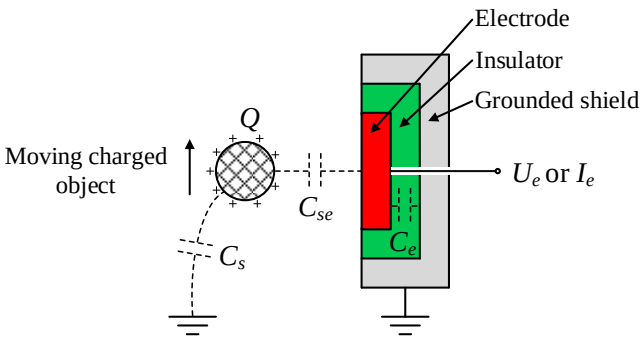

Fig. 1. Schematic diagram of an electrode used for sensing of a charged object moving in space.

II. Circuit Models of Electrostatic Sensors

A. Equivalent Circuit Model of the Electrode

The motion of a charged object gives rise to redistribution of electrons in the electrode, therefore most studies on modelling of electrostatic sensors have focused on calculation of the induced charge by means of mathematical modelling [12, 18, 19] or finite element simulation [11, 21]. The amount of induced charge is dependent on the location of the charged object relative to the electrode. In order to quantify this effect, a dimensionless index named spatial sensitivity has been defined as the ratio between the induced charge and the source charge at a given location in space. On the other hand, electric field coupling is also known as capacitive coupling, so the electrostatic interaction between the charged object and the electrode can also be quantified using capacitance [13, 22]. Similar to the spatial sensitivity, the capacitance between the charged object and the electrode is dependent on the relative location of the charged object. It should be noted that electrostatic sensors behave like capacitive sensors, as both work on the principle of electric field sensing. However, they are different because electrostatic sensors exploit the passively generated electric field due to the moving charged object, while most capacitive sensors generate actively a fluctuating electric field. As a result, most readout circuits of capacitive sensors cannot be used for electrostatic sensors.

Fig. 1 shows a schematic diagram of an electrode used for sensing of a charged object moving in space. The electrode is embedded in a grounded metal shield via a sandwiched insulator to reject external electromagnetic interference. The capacitance between the electrode and the shield, represented by C_e, is dependent on the thickness, area and permittivity of the insulator. The charged object develops an electric potential due to the capacitance C_s between the object and the ground (the subscript *s* is used because the charged object is the source of the electric field). The object-electrode capacitance C_{se} changes as the charged object moves relative to the electrode.

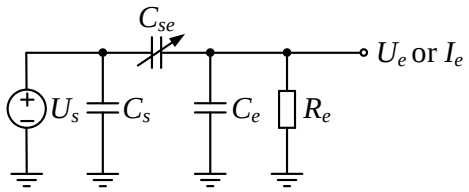

Fig. 2. Equivalent circuit model of the electrode.

The capacitive coupling model of the electrode shown in Fig. 1 allows for analysis using classical circuit theory. Fig. 2 shows an equivalent circuit model of the electrode. The potential of the charged object is expressed as

$$U_s = \frac{Q}{C_s} \tag{1}$$

where Q is the amount of charge on the object. Assuming that the object has been charged to a saturate level and its motion does not change the capacitance C_s considerably, then the potential of the object remains almost constant. As the object moves in space, the object-electrode capacitance C_{se} is a function of time and thus represented using a variable capacitor in the equivalent circuit. The insulation resistance of the electrode is represented by R_e. The output of the electrode is either a voltage signal U_e or a current signal I_e, depending on whether the electrode is driven to a fixed potential by the preamplifier.

B. Preamplifiers

For the sake of convenience, phasor representation is used to analyze the following four types of preamplifiers.

(1) Trans-resistance Amplifier

The trans-resistance amplifier is also termed as current-to-voltage converter or simply I/V converter. It is the most used analog front end for signal conditioning of electrostatic sensors [6, 11, 17-22]. As shown in Fig. 3, the electrode is connected to the inverting terminal of an operational amplifier via a coaxial cable. Because the electrode is held at virtual ground by the negative feedback of the operational amplifier, the variable object-electrode capacitance results in induced current I_e which is expressed as

$$I_e = j\omega C_{se} U_s \tag{2}$$

In Fig. 3, the stray capacitance of the cable is represented by C_c, and the input capacitance and input resistance of the operational amplifier are represented by C_{in} and R_{in}, respectively. Because the potential difference across C_e, R_e, C_c, C_{in} and R_{in} is zero, the induced current does not flow through these components and their effects are neglected.

The trans-resistance amplifier converts the induced current into a voltage signal using a large valued feedback resistor R_f. In order to improve stability, a small valued capacitor C_f is placed in parallel with the feedback resistor. The output voltage U_o of the trans-resistance amplifier is expressed as

$$U_o = -\frac{R_f I_e}{1 + j\omega R_f C_f} \tag{3}$$

Substituting (2) into (3) yields

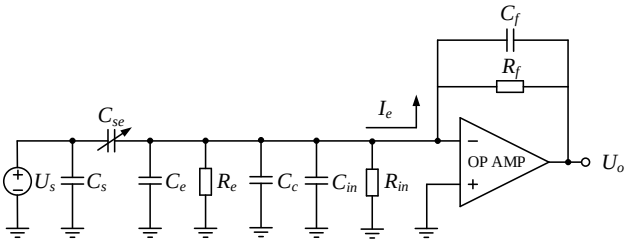

Fig. 3. Circuit of the trans-resistance amplifier and the charge amplifier.

$$U_o = -\frac{j\omega R_f C_{se}}{1 + j\omega R_f C_f} U_s \tag{4}$$

It can be seen from (4) that the output voltage is dependent on the object-electrode capacitance C_{se} and its rate of change represented by the angular frequency ω.

Normally, the feedback resistor R_f is in the order of tens to hundreds of MΩ while the feedback capacitor C_f is in the order of several pF, so the impedance of R_f is much smaller than that of C_f for ω from zero to several kHz. Consequently, the induced current mainly passes through R_f. In the low frequency band that electrostatic sensors normally operate within, the condition $\omega R_f C_f \ll 1$ leads to the following simplification of (4)

$$U_o = -j\omega R_f C_{se} U_s \tag{5}$$

Equation (5) shows that the gain of the trans-resistance amplifier is determined by R_f. As the operating frequency of the electrostatic sensor increases, the effect of C_f becomes more pronounced, leading to waveform distortion of the output signal.

(2) Charge Amplifier

The charge amplifier is essentially a current integrator that produces a voltage signal proportional to the integrated value of the input current [7, 8, 12, 17, 30]. A charge amplifier working in AC mode has the same circuit configuration as that of a trans-resistance amplifier [23], as shown in Fig. 3. Therefore, the output voltage is also described by (4). However, the functions and values of the feedback resistor and the feedback capacitor are completely different. The value of the feedback capacitor is commonly larger than that in the trans-resistance amplifier. The induced current is accumulated on the feedback capacitor which develops the output voltage. The feedback resistor continuously bleeds off the accumulated charge on the feedback capacitor in order to prevent the charge amplifier from drifting into saturation due to the leakage current at the input terminal of the operational amplifier. The value of the feedback resistor is usually in the order of GΩ, so that the discharge rate of the feedback capacitor is very low and the amplitude response at low frequencies is attenuated only slightly.

When the values of the feedback capacitor and the feedback resistor are sufficiently large and the condition $\omega R_f C_f \gg 1$ is satisfied, (4) is simplified as

$$U_o = -\frac{C_{se}}{C_f} U_s \tag{6}$$

It is obvious that the gain of the charge amplifier is determined by the feedback capacitor.

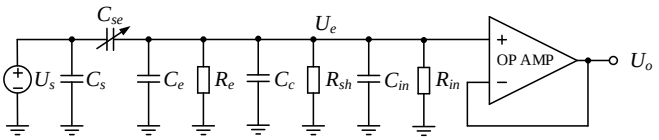

Fig. 4. Circuit of the current sense amplifier.

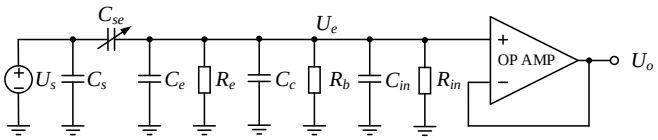

Fig. 5. Circuit of the potential amplifier.

(3) Current Sense Amplifier

The current sense amplifier is also referred to as current shunt amplifier, which measures the current by placing a shunt resistor in the current path [9, 10, 28]. As shown in Fig. 4, the electrode is connected to the ground by a shunt resistor R_{sh} and the voltage drop developed across R_{sh} by the induced current is buffered using a unity-gain amplifier that provides impedance transformation. Because C_e, R_e, C_c, C_{in} and R_{in} are in parallel with R_{sh}, their effects cannot be ignored any longer. A capacitive voltage divider is formed by the object-electrode capacitance C_{se} together with the capacitors and resistors at the input terminal of the buffer amplifier. The output voltage of the current sense amplifier is expressed as

$$U_o = \frac{j\omega R_e R_{sh} R_{in} C_{se}}{R_{sh}R_{in} + R_e R_{sh} + R_e R_{in} + j\omega R_e R_{sh} R_{in}(C_{se} + C_e + C_c + C_{in})} U_s \quad (7)$$

Equation (7) can be transformed into

$$U_o = \frac{j\omega C_{se}}{\frac{1}{R_e} + \frac{1}{R_{in}} + \frac{1}{R_{sh}} + j\omega(C_{se} + C_e + C_c + C_{in})} U_s \quad (8)$$

Because the shunt resistor R_{sh} is in the order of MΩ and much smaller than R_e and R_{in}, the first two terms in the denominator of (8) can be ignored, which yields

$$U_o = \frac{j\omega R_{sh} C_{se}}{1 + j\omega R_{sh}(C_{se} + C_e + C_c + C_{in})} U_s \quad (9)$$

In addition, the capacitors C_{se}, C_e, C_c and C_{in} are in the order of pF, so the second term in the denominator of (9) can be ignored at low frequencies. Then the expression of the output voltage is simplified as

$$U_o = j\omega R_{sh} C_{se} U_s \quad (10)$$

It is worth noting that because the trans-resistance amplifier and the current sense amplifier both measure the induced current using a resistor, (5) and (10) are similar in form except for the sign of the output voltage. Different from the trans-resistance amplifier, the capacitors C_e, C_c and C_{in} at the input affect the frequency response of the current sense amplifier, especially at high frequencies, as illustrated by (9).

(4) Potential Amplifier

The potential amplifier is simply a unity-gain amplifier that buffers the potential of the electrode developed as a result of the induced charge on the electrode and the capacitance between the electrode and the ground [13-15], as shown in Fig. 5. In order to provide a path for the input bias current of the operational amplifier, the non-inverting terminal is connected to ground using a large valued bias resistor R_b, through which the induced current from the electrode barely flows. The bias resistor degrades the input impedance of the buffer amplifier. In order to solve this issue, two back-to-back diodes with ultra-low leakage current can be used to replace R_b [24] or the bootstrapping technique can be used to increase the apparent input impedance [25]. With the biasing scheme shown in Fig. 5, the output voltage is expressed as

$$U_o = \frac{j\omega R_e R_b R_{in} C_{se}}{R_b R_{in} + R_e R_b + R_e R_{in} + j\omega R_e R_b R_{in}(C_{se} + C_e + C_c + C_{in})} U_s \quad (11)$$

Because R_e, R_{in} and R_b are all very large, (11) is simplified as

$$U_o = \frac{C_{se}}{C_{se} + C_e + C_c + C_{in}} U_s \quad (12)$$

Equation (12) shows that the magnitude of the output voltage is affected by the capacitors C_e, C_c and C_{in} at all frequencies. All frequency components of the source signal are amplified with the same gain and the same phase shift, so the shape of the source signal is unaffected. In order to enhance the sensitivity of the sensor, active guarding and neutralization techniques have been used to reduce the capacitances at the input terminal [26].

III. Experimental Results

A. Experimental Setup

In order to conduct experimental comparison of the preamplifiers, repeatable inputs to the electrostatic sensor should be generated. There exist a few approaches for experimental assessment of electrostatic sensors in the laboratory. Because the passage of the charged object through the sensing area of the electrode can be regarded as an impulse input, free-fall of a dielectric particle is commonly used to obtain the impulse response of the electrostatic sensor [17, 27, 28]. However, the repeatability of this method is low, as the amount of charge on the particle is uncertain. For investigation of the frequency response, a continuously fluctuating electric field can be generated using a power transmission belt [11, 12, 29] or pneumatically conveyed particle flow [10, 20, 21, 28, 29]. But the fluctuation of the electric field is stochastic in nature and the experiments cannot be repeated at all.

As explained, the signal of the electrostatic sensor is generated due to the variation of the object-electrode capacitance C_{se}. The multiplication of C_{se} with U_s in the equations of the output voltage implies that the input to the electrostatic sensor can also be generated by varying U_s while keeping C_{se} constant. It is much easier and more convenient to apply a varying voltage signal on an emitting electrode to generate a fluctuating electric field than the aforementioned experimental methods. The amplitude, frequency, phase and waveform of the voltage signal can be precisely controlled, leading to high repeatability of the experimental results. Moreover, the applied voltage signal can be an impulse, periodic or stochastic signal, and even real-world signals collected from the industrial field can be reproduced.

Fig. 6 shows a schematic diagram of the experimental setup. A data acquisition device (DAQ, USB-6212, National

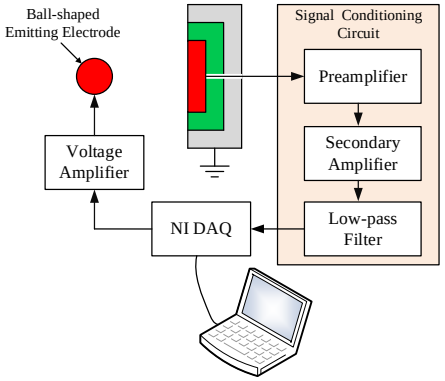

Fig. 6. Schematic diagram of the experimental setup.

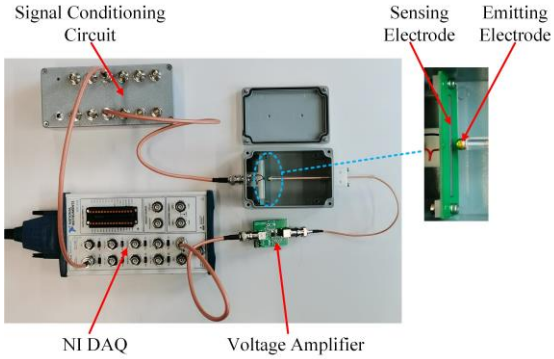

Fig. 7. Photo of the experimental setup.

Instruments) is used to generate a voltage signal in the range from 0 V to 5 V. The voltage signal is amplified to the range from 0 V to 60 V using a voltage amplifier powered from a DC 64 V supply. Then the signal is applied on a ball-shaped emitting electrode with a diameter of 6 mm. A strip-shaped sensing electrode with dimensions of 4 mm × 48 mm is placed 6 mm away from the center of the emitting electrode. The sensing electrode is connected to the signal conditioning circuit via a coaxial cable with a length of 0.5 m. The outer shield conductor of the coaxial cable is grounded at both ends via Bayonet Neill-Concelman (BNC) connectors. The electrodes and the signal conditioning circuit are enclosed separately in two aluminum shielding cases to reject external electromagnetic interference. The output of the signal conditioning circuit is then sampled into a computer using the DAQ at a rate of 200 kHz. Fig. 7 shows a photo of the experimental setup.

Fig. 8 shows the signal conditioning circuits fixed inside the aluminum case. The four types of preamplifiers are the first stages of the signal conditioning circuits. The feedback resistor of the trans-resistance amplifier and the shunt resistor of the current sense amplifier are both 10 MΩ. The feedback capacitor of the trans-resistance amplifier is 10 pF. The feedback capacitor and the feedback resistor of the charge amplifier are 100 pF and 2 GΩ, respectively. The potential amplifier is biased using BAV199 (Nexperia) that integrates a pair of back-to-back low-leakage diodes. Moreover, in order to reduce the effects of input capacitances on the signals of the current sense amplifier and the potential amplifier, two extra circuit boards with active guarding and triaxial connectors were developed (the two rightmost circuit boards in Fig. 8). The second stages of the signal conditioning circuits are non-inverting amplifiers with the same voltage gain of 25.9,

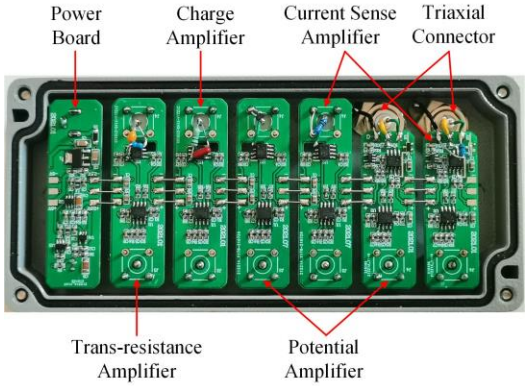

Fig. 8. Signal conditioning circuits.

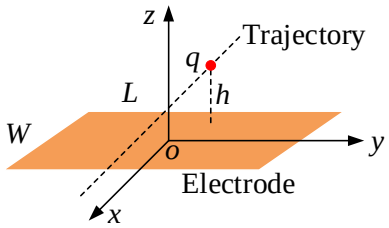

Fig. 9. Charge induction on a strip-shaped electrode by a charged particle.

and the third stages are Sallen-Key low-pass filters with the same cut-off frequency of 10 kHz. A dedicated power board supplies ±2.5 V DC power for the signal conditioning circuits.

B. Impulse Response

When monitoring the movement of charged objects using electrostatic sensors, the electrode is typically placed in parallel with the moving direction of the object, although in practice pneumatically conveyed particles may move in an oblique direction and power transmission belts may vibrate transversely. Because such unusual cases generate unsymmetric or even erratic inputs to electrostatic sensors that are not amenable for quantitative analysis, an ideal case of a small charged particle travelling along a line trajectory in parallel with a strip-shaped electrode as shown in Fig. 9 is considered. The induced charge on the electrode is of impulsive nature and given by [30]

$$q'(t) = -\frac{q}{\pi}\{\arctan[\frac{\frac{L}{2}(\frac{W}{2}-vt)}{h\sqrt{(\frac{W}{2}-vt)^2+\frac{L^2}{4}+h^2}}) + \arctan(\frac{\frac{L}{2}(\frac{W}{2}+vt)}{h\sqrt{(\frac{W}{2}+vt)^2+\frac{L^2}{4}+h^2}}]\} \quad (13)$$

where q is the quantity of charge carried on the particle, L is the electrode length, W is the electrode width, h is the distance between the line trajectory and the electrode plane, and v is the velocity of the charged particle. The pulse-like voltage applied on the emitting electrode is described by the following equation that is adapted from (13)

$$U(t) = A\{\arctan[\frac{\frac{L}{2}(\frac{W}{2}-vt)}{h\sqrt{(\frac{W}{2}-vt)^2+\frac{L^2}{4}+h^2}}) + \arctan(\frac{\frac{L}{2}(\frac{W}{2}+vt)}{h\sqrt{(\frac{W}{2}+vt)^2+\frac{L^2}{4}+h^2}}]\} \quad (14)$$

where A determines the magnitude of the pulse-like voltage.

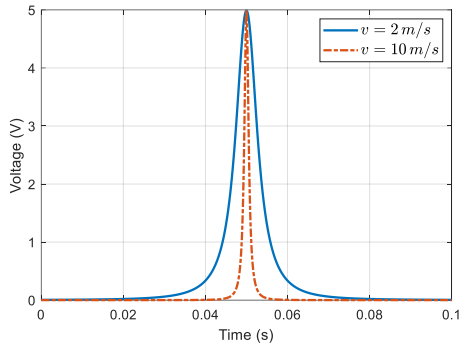

Fig. 10. Impulse excitation signals from the DAQ for *v*=2 m/s and 10 m/s. Parameters: *A*=8 V, *L*=0.048 m, *W*=0.004 m, *h*=0.006 m.

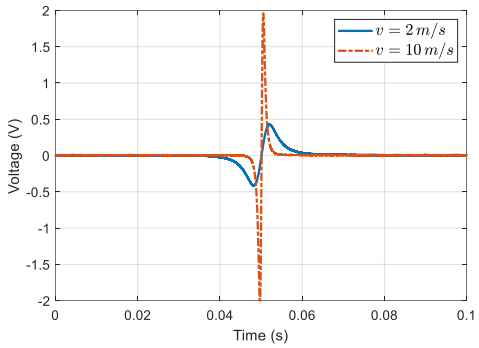

Fig. 11. Impulse response of the trans-resistance amplifier.

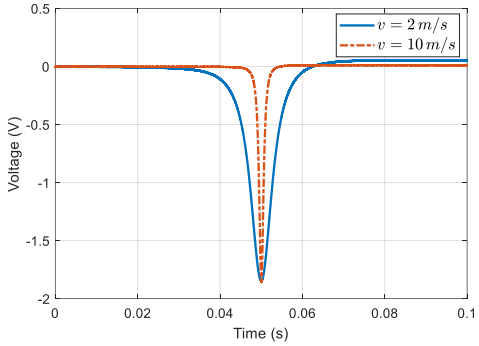

Fig. 12. Impulse response of the charge amplifier.

Fig. 10 plots the waveforms of two impulse excitation signals calculated using equation (14), when the velocity of the charged particle is 2 m/s and 10 m/s, respectively. It can be seen that as the velocity increases, the voltage pulse becomes narrower. However, the pulse magnitude remains unchanged regardless of the velocity.

Fig. 11 shows the impulse response of the trans-resistance amplifier. When the charged particle is simulated to approach the electrode, the electrons flow from the electrode to the virtual ground. As the charged particle moves away, the electrons flow back in the opposite direction. Therefore, the sensor signal is bipolar, exhibiting first negative and then positive polarities. The waveform of the signal is almost symmetrical about the point that corresponds to the closest distance between the charged particle and the electrode. In addition, a larger velocity of the charged particle leads to a higher peak magnitude of the signal.

Fig. 12 illustrates the impulse response of the charge amplifier. Because the output voltage of the charge amplifier is proportional to the total induced charge on the electrode, the sensor signal is basically unipolar in the form of a negative pulse. It is noticeable that the signal for the low velocity has a long tail. This is because at low frequencies the impedance of the feedback capacitor is higher and more current flows through the feedback resistor than at high frequencies. In this case, the charge amplifier tends to degenerate into a trans-resistance amplifier and hence the signal waveform tends to resemble those in Fig. 11. Additionally, the velocity of the point change does not affect the peak magnitude of the signal.

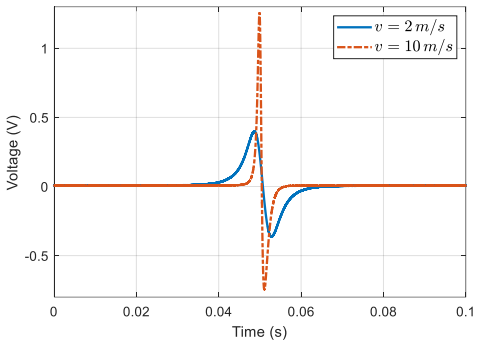

Fig. 13. Impulse response of the current sense amplifier.

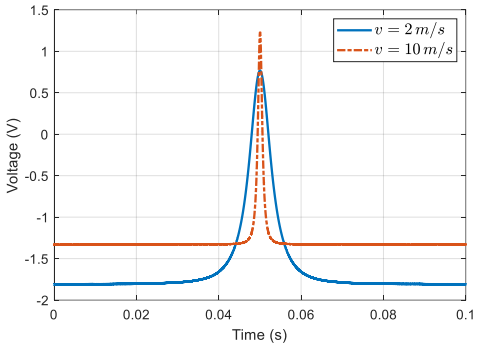

Fig. 14. Impulse response of the potential amplifier.

Fig. 13 illustrates the impulse response of the current sense amplifier. The signal is also bipolar, but the polarity is opposite to that of the trans-resistance amplifier, which can be explained by the opposite signs in equations (5) and (10). The waveform of the signal is no longer symmetrical about the point with zero current, and this phenomenon is more obvious for the high velocity. It can be explained that at high frequencies the impedance of the parasitic capacitors C_e, C_c and C_{in} at the input of the amplifier is lower and more current flows through the parasitic capacitors than at low frequencies. In this case, the signal waveform of the current sense amplifier tends to resemble that of a potential amplifier, as will be described below. Another difference from the trans-resistance amplifier is the smaller magnitude of the signal due to the influence of the parasitic capacitors, even though the feedback resistor of the trans-resistance amplifier and the shunt resistor of the current sense amplifier have the same value.

Fig. 14 illustrates the impulse response of the potential amplifier. Different from all above preamplifiers, the DC voltage of the potential amplifier is not stable and it takes a very long time (in the order of minutes) for the output to settle down

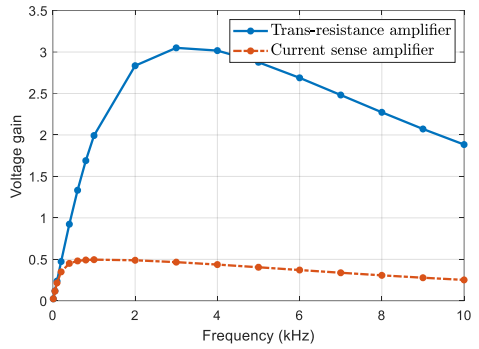

Fig. 15. Voltage gains obtained using the trans-resistance amplifier and the current sense amplifier.

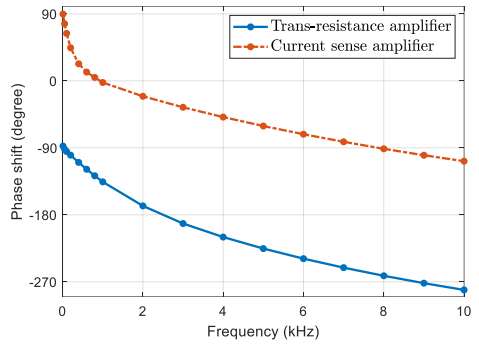

Fig. 16. Phase shifts obtained using the trans-resistance amplifier and the current sense amplifier.

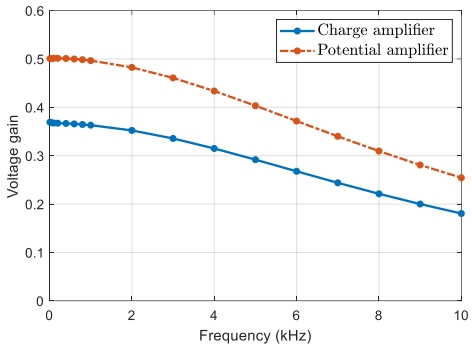

Fig. 17. Voltage gains obtained using the charge amplifier and the potential amplifier.

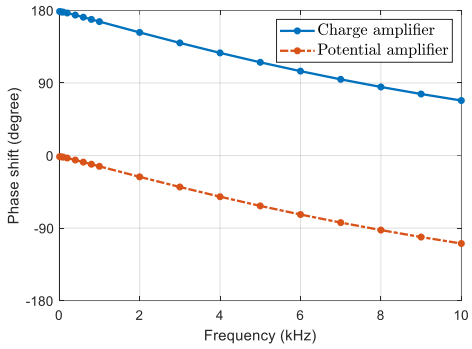

Fig. 18. Phase shifts obtained using the charge amplifier and the potential amplifier.

after power on. The reason for this is that the input impedance of the potential amplifier is very high and the electrode is electrically floating. Reducing the input impedance using back-to-back diodes with larger leakage current can shorten the settling time, but the potential amplifier tends to degenerate into the current sense amplifier. Neglecting the DC component, the signal waveform of the potential amplifier is similar to that of the charge amplifier, except for the polarity.

C. Frequency Response

In order to investigate the frequency response of the electrostatic sensor, a sinusoidal excitation signal described by the following equation is generated using the DAQ

$$U(t) = A + A\sin(2\pi ft + \varphi) \tag{15}$$

where A is the amplitude, f is the frequency, and φ is the initial phase that is set as -90 degrees in order for the signal to start from zero volt. The frequency sweeps from 10 Hz to 10 kHz with a variable step, so that the voltage gains and the phase shifts at different frequencies are obtained.

The magnitude response is evaluated by calculating the voltage gain of the sensor signal with reference to the DAQ output. Fig. 15 plots the voltage gains obtained using the trans-resistance amplifier and the current sense amplifier. Both voltage gains increase linearly with the frequency at low frequencies and then decrease at high frequencies because of the attenuation effects of the Sallen-Key low-pass filters. The voltage gain obtained using the current sense amplifier starts to decline at a lower frequency than that obtained using the trans-resistance amplifier due to the parasitic capacitances at the input. Except for the low frequencies, the voltage gain of the current sense amplifier is smaller than that of the trans-resistance amplifier, despite of the same current measuring resistors.

Fig. 16 shows the phase shifts obtained using the trans-resistance amplifier and the current sense amplifier. At low frequencies, the phase shifts with respect to the excitation signal are approximately -90 and 90 degrees, respectively. As the frequency increases, the low-pass filters cause increasing phase lags. The phase shift of the current sense amplifier decreases more quickly than that of the trans-resistance amplifier at low frequencies due to the parasitic capacitances.

Fig. 17 shows the voltage gains obtained using the charge amplifier and the potential amplifier. The waveforms of the two curves are very alike, both decreasing with the frequency due to the low-pass filters. Different from the current sense amplifier, the influence of the parasitic capacitances on the voltage gain of the potential amplifier does not change with the frequency, because the voltage gain is determined by capacitive divider described by equation (12). It should be noted that the voltage gains of the charge amplifier and the potential amplifier should not be compared with each other, because they are determined by different components of the circuits.

Fig. 18 depicts the phase shifts obtained using the charge amplifier and the potential amplifier. At low frequencies, the phase shifts are about 180 degrees and 0 degree, respectively. The descending rates of the phase shifts are similar, suggesting that the influence of the parasitic capacitances is negligible and the phase lags are caused purely by the low-pass filters.

The frequency response obtained above is useful for understanding the behaviors of the preamplifiers at different frequencies. Such knowledge is important for selecting the right preamplifier for the target application. For instance, in

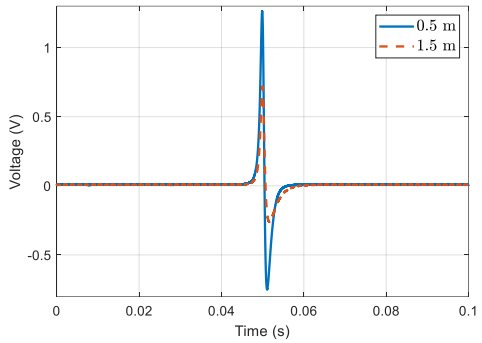

Fig. 19. Impulse response of the current sense amplifier obtained using coaxial cables of different lengths.

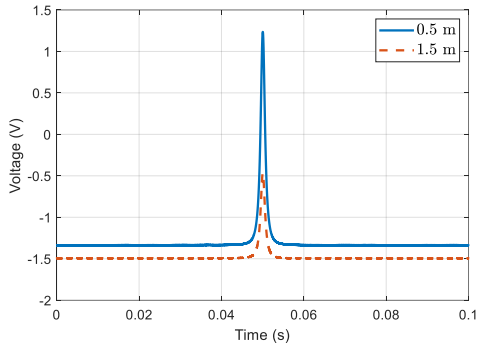

Fig. 20. Impulse response of the potential amplifier obtained using coaxial cables of different lengths.

gas–solid two-phase flow measurement [6], the particle velocity determines the frequency of the fluctuating electric field for a given electrode. If a trans-resistance amplifier or a current sense amplifier is used, the particle velocity affects the signal amplitude which is usually used to measure the volumetric concentration. On the contrary, the signal amplitude of a charge amplifier or a potential amplifier is not affected by the particle velocity. For vibration monitoring of power transmission belts [12], the phase of the signal is useful for deciding whether the belt is approaching or moving away from the sensor.

D. Mitigating Effect of Parasitic Capacitances

The experimental results presented above show that the parasitic capacitances at the input of the current sense amplifier and the potential amplifier have significant effects on the impulse and frequency responses, whereas the trans-resistance amplifier and the charge amplifier are barely affected. Therefore, measures should be taken to mitigate the effects of parasitic capacitances when using the current sense amplifier and the potential amplifier.

The electrode-ground capacitance C_e is determined by the structural design of the electrostatic sensor. For a ring-shaped electrode for pulverized coal flow metering in power stations [6], the electrode-ground capacitance can be as large as several nF. The thickness, area and permittivity of the insulator material should be properly designed in order to reduce the electrode-ground capacitance.

Since the stray capacitance of the coaxial cable is affected by its length, the responses of the current sense amplifier and the potential amplifier change when using coaxial cables of different lengths. Fig. 19 and Fig. 20 show that the peak magnitudes of the sensor signals obtained using the current sense amplifier and the potential amplifier are reduced considerably when the cable length is increased from 0.5 m to 1.5 m. The difference between the peak magnitudes of the positive and negative pulses in Fig. 19 is also enlarged when increasing the cable length. In order to mitigate the effects of cable length, triaxial cables with an inner shield conductor driven to the potential of the preamplifier output should be used. Fig. 21 and Fig. 22 show the impulse responses of the current sense amplifier and the potential amplifier using triaxial cables of different lengths, respectively. As can be seen, the cable length has virtually no influence on the impulse responses and the sensor signals are stronger than those obtained using coaxial cables shown in Fig. 19 and Fig. 20. Particularly, the potential amplifier has very high voltage gain because of the extremely high input impedance.

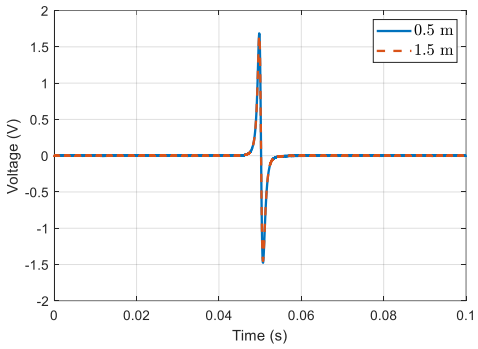

Fig. 21. Impulse response of the current sense amplifier obtained using triaxial cables of different lengths.

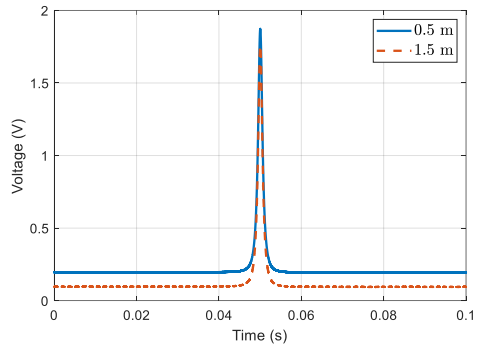

Fig. 22. Impulse response of the potential amplifier obtained using triaxial cables of different lengths. Note that the voltage gain of the non-inverting amplifier at the second stage of the conditioning circuit has been reduced from 25.9 to 6.0 in order to prevent the output from hitting the +2.5V power rail.

The trace of the electrode signal on the PCB of the signal conditioning circuit is another source of stray input capacitance. The trace should be kept as short as possible. As mentioned, the active guarding and neutralization techniques can also help reduce the input capacitance for a potential amplifier.

IV. Conclusion

This paper has presented an equivalent circuit model of the electrostatic sensor that comprehensively takes into account the charged object, the electrode and the preamplifier. In

comparison with the common modelling approach that calculates induced charge and spatial sensitivity of the electrode, the proposed modelling approach allows for analysis of the entire sensor using classical circuit theory. The voltage outputs of the electrostatic sensor with four types of preamplifiers have been derived analytically. In order to produce repeatable and controllable inputs to the electrostatic sensor for experimental comparison, an electric field is actively generated using an emitting electrode driven by a controlled voltage signal. Both impulse and frequency responses of the electrostatic sensor are obtained experimentally. The results have demonstrated that the trans-resistance amplifier and the current sense amplifier yield similar signal waveforms apart from the opposite polarities whereas the charge amplifier and the potential amplifier behave similarly. The current sense amplifier and the potential amplifier are significantly affected by the parasitic capacitances at the input, which require special measures to minimize such an effect. By contrast, the trans-resistance amplifier and the charge amplifier are immune to the parasitic capacitors that are virtually short-circuited by the operational amplifier. Nevertheless, it is recommended to keep the cable between the electrode and the preamplifier as short as possible because of non-ideal characteristics of the operational amplifier. The potential amplifier is particularly recommended to use when conditioning extremely weak signals, as long as guarding, shielding and neutralization measures are properly implemented.

The experimental results presented in this paper were obtained under laboratory conditions. In future work, experimental tests will be conducted to compare the preamplifiers in real-world settings, such as pulverized coal flow metering in power stations [6]. The guidelines for cabling and electrode design will also be validated using field test results.

REFERENCES

[1] F. Chowdhury, M. Ray, A. Sowinski, P. Mehrani, and A. Passalacqua, "A review on modeling approaches for the electrostatic charging of particles," *Powder Technol*., vol. 389, pp.104-118, 2021.

[2] T. I. Lekas, "Electrostatic charging of an aircraft due to airborne dust particles impacts," *CEAS Aeronaut. J*., vol. 10, pp. 903-908, 2019.

[3] D. J. Breton, N. J. Lamie and E. Asenath-Smith, "Triboelectric charge variability in firearm particulates and projectiles," *J. Electrostat.*, vol. 89, pp. 13-19, 2017.

[4] Y. Yan, Y. Hu, L. Wang, X. Qian, W. Zhang, K. Reda, J. Wu and Ge Zheng, "Electrostatic sensors - Their principles and applications," *Measurement*, vol. 169, 2021, Art. no. 108506.

[5] T. Tajdari, M. F. Rahmat, N. A. Wahab and I. T. Thuku, "Low noise signal conditioning design for electrostatic sensors," *Sens. Transd.*, vol. 153, no. 6, pp. 200-208, 2013.

[6] X. Qian, Y. Yan, X. Huang and Y. Hu, "Measurement of the mass flow and velocity distributions of pulverized fuel in primary air pipes using electrostatic sensing techniques," *IEEE Trans. Instrum. Meas.*, vol. 66, no. 5, pp. 944-952, 2017.

[7] H. Mao, H. Zuo and H. Wang, "Electrostatic sensor application for on-line monitoring of wind turbine gearboxes," *Sensors*, vol. 18, no. 9, 2018, Art. no. 3574.

[8] T. Addabbo, A. Fort, M. Mugnaini, E. Panzardi and V. Vignoli, "A smart measurement system with improved low-frequency response to detect moving charged debris," *IEEE Trans. Instrum. Meas.*, vol. 70, no. 8, pp. 1874-1883, 2016.

[9] M. F. Rahmat, I. T. Thuku, T. Tajdari, K. Jusoff and M. R. Ghazali, "Sensing and filtering characteristics of electrostatic sensors for pneumatically conveyed particles," *Int. J. Phys. Sci.*, vol. 62, no. 22, pp. 5091-5103, 2011.

[10] C. Xu, B. Zhou and S. Wang, "Dense-phase pneumatically conveyed coal particle velocity measurement using electrostatic probes," *J. Electrostat.*, vol. 68, pp. 64-72, 2010.

[11] Y. Hu, Y. Yan, L. Wang and X. Qian, "Non-contact vibration monitoring of power transmission belts through electrostatic sensing," *IEEE Sens. J.*, vol. 16, no. 10, pp. 3541-3550, 2016.

[12] Y. Hu, S. Zhang, Y. Yan, L. Wang, X. Qian and Lu Yang, "A smart electrostatic sensor for online condition monitoring of power transmission belts," *IEEE Trans. Ind. Electron.*, vol. 64, no. 9, pp. 7313-7322, 2017.

[13] J. B. Gajewski, "Frequency response and bandwidth of an electrostatic flow probe," *J. Electrostat*., vol. 48, pp. 279-294, 2000.

[14] S. Wang, L. Zhang, F. Sun, Z, Dong, F. Yan and X. Yang, "A recognition method for hand motion direction based on charge induction," *IEEE Sens. J.*, vol. 20, no. 1, pp. 415-424, 2020.

[15] C. A. Browning, S. J. Vinci, J. Zhu, D. M. Hull and M. A. Noras, "An evaluation of electric-field sensors for projectile detection," *Proc. 2013 IEEE Sens.*, Baltimore, MD, USA, 3-6 Nov. 2013, pp. 1-4.

[16] Y Sun and X. Yu, "Capacitive biopotential measurement for electrophysiological signal acquisition: A review," *IEEE Sens. J.*, vol. 16, no. 9, pp. 2832-2853, 2017.

[17] C. Wang, Y. Li, L. Jia, S. Zhang and J. Ye, "Design of charge-sensitive and current-sensitive preamplifiers for electrostatic sensor," *J. Electrostat.*, vol. 105, 2020, Art. no. 103449.

[18] S. N. Murnane, R. N. Barnes, S. R. Woodhead and J. E. Amadi-Echendu, "Electrostatic modelling and measurement of airborne particle concentration," *IEEE Trans. Instrum. Meas.*, vol. 45, no. 2, pp. 488-492, 1996.

[19] Z. Chen, X. Tang, Z. Hu and Y. Yang, "Investigations into sensing characteristics of circular thin-plate electrostatic sensors for gas path monitoring," *Chinese J. Aeronaut.*, vol. 27, no. 4, pp. 812-820, 2014.

[20] W. Zhang, Y. Yan, Y. Yang and J. Wang, "Measurement of flow characteristics in a bubbling fluidized bed using electrostatic sensor arrays," *IEEE Trans. Instrum. Meas.*, vol. 65, no. 3, 703-712, 2016.

[21] Z. Wen, X. Ma, H. Zuo, "Characteristics analysis and experiment verification of electrostatic sensor for aero-engine exhaust gas monitoring," *Measurement*, vol. 47, pp. 633-644, 2014.

[22] K. Kurita and S. Morinaga, "Noncontact detection of movements of standing up from and sitting down on a chair using electrostatic induction," *IEEE Sens. J.*, vol. 19, no. 19, pp. 8934-8939, 2019.

[23] G. Gautschi. Piezoelectric Sensorics, Springer, 2002.

[24] Y. M. Chi, S. R. Deiss and G. Cauwenberghs, "Non-contact low power EEG/ECG electrode for high density wearable biopotential sensor networks," *Proc. Sixth Int. Workshop on Wearable and Implantable Body Sensor Networks, Berkeley*, CA, USA, 3-5 Jun. 2009, pp. 246-250.

[25] E. Spinelli, F. Guerrero, P. Garcíaa and M. Haberman, "A simple and reproducible capacitive electrode," *Med. Eng. Phys.*, vol. 38, pp. 286-289, 2016.

[26] Y. M. Chi and G. Cauwenberghs, "Micropower non-contact EEG electrode with active common-mode noise suppression and input capacitance cancellation," *Proc. 2009 Annu. Int. Conf. IEEE Engineering in Medicine and Biology Society*, Minneapolis, MN, USA, 3-6 Sept. 2009, pp. 4218-4221.

[27] T. Tajdari, M. F. Rahmat and N. A. Wahab, "New technique to measure particle size using electrostatic sensor," *J. Electrostat.*, vol. 72, no. 2, pp. 120-128, 2014.

[28] C. Xu, S. Wang, G. Tang, D. Yang and B. Zhou, "Sensing characteristics of electrostatic inductive sensor for flow parameters measurement of pneumatically conveyed particles," *J. Electrostat.*, vol. 65, no. 9, pp. 582-592, 2007.

[29] C. Wang, J. Zhang, W. Gao, H. Ding and W. Wu, "Cross-correlation focus method with an electrostatic sensor array for local particle velocity measurement in dilute gas–solid two-phase flow," *Meas. Sci. Technol.*, vol. 26, 2015, Art. no. 115301.

[30] D. I. Armour-Chelu, S. R. Woodhead and R. N. Barnes. "The electrostatic charging trends and signal frequency analysis of a particulate material during pneumatic conveying," *Powder Technol.*, vol. 96, pp. 181-189, 1998.

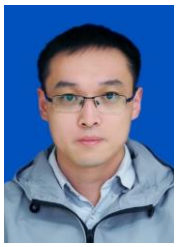

Yonghui Hu (Senior Member, IEEE) received the B.Eng. degree in automation from Beijing Institute of Technology, Beijing, China, in 2004, and the Ph.D. degree in dynamics and control from Peking University, Beijing, in 2009.

He was a Post-Doctoral Research Fellow with Beihang University, Beijing, from 2010 to 2012, and a Research Associate with University of Kent, Canterbury, U.K., from 2019 to 2021. He is currently an Associate Professor with the School of Control and Computer Engineering, North China Electric Power University, Beijing. His current research interests include multiphase flow measurement and condition monitoring of various industrial processes.

Yong Yan (Fellow, IEEE) received the B.Eng. and M.Sc. degrees in instrumentation and control engineering from Tsinghua University, Beijing, China, in 1985 and 1988, respectively, and the Ph.D. degree in flow measurement and instrumentation from the University of Teesside, Middlesbrough, U.K., in 1992.

He was an Assistant Lecturer with Tsinghua University in 1988. In 1989, he joined the University of Teesside as a Research Assistant. After a short period of Post-Doctoral Research, he was a Lecturer with the University of Teesside from 1993 to 1996, and then as a Senior Lecturer, a Reader, and a Professor with the University of Greenwich, Chatham, U.K., from 1996 to 2004. He is currently a Professor of electronic instrumentation and the Director of innovation at the School of Engineering and Digital Arts, the University of Kent, Canterbury, U.K. His current research interests include multiphase flow measurement, combustion instrumentation, and intelligent measurement and condition monitoring.

Dr. Yan was elected as a Fellow of the Royal Academy of Engineering in 2020. He was awarded the gold medal in 2020 by the IEEE TRANSACTIONS ON INSTRUMENTATION AND MEASUREMENT as the most published author of all time from the U.K.

Yuanqing Yang received the B.Eng. and M.Sc. degrees in control science and engineering from North China Electric Power University, Beijing, China, in 2019 and 2022, respectively.

She is currently an engineer with State Power Investment Corporation Limited, China. Her research interests include multiphase flow monitoring techniques and digital signal processing.